AD-A146 276 EFFECTS OF PRIOR AUSTENITE AND FERRITE GRAIN SIZE ON FRACTURE PROPERTIES O.. (U) BROWN UNIV PROVIDENCE RI DIV OF ENGINEERING H COUQUE ET AL. 01 JUL 84 1/1

UNCLASSIFIED ARO-18414.6-EG DAAG29-81-K-0121 F/G 11/6 NL

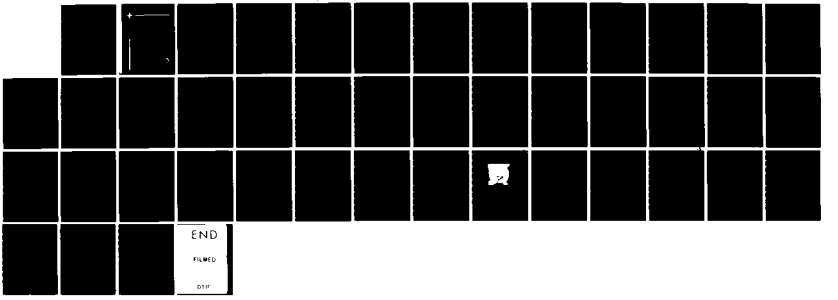

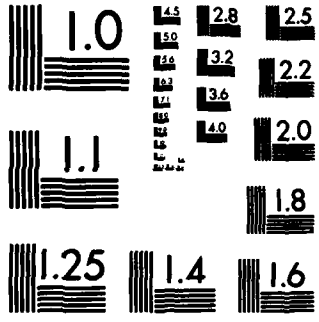

ARO 18414.6-EG

Brown University
DIVISION OF ENGINEERING
PROVIDENCE, R.I. 02912

(2)

Effects of Prior Austenite and Ferrite Grain Size on Fracture Properties of a Plain Carbon Steel

by

H. Couque, J. Duffy and R.J. Asaro

Division of Engineering
Brown University

84 09 25 133

UNCLASSIFIED
SECURITY CLASSIFICATION OF THIS PAGE (When Data Entered)

REPORT DOCUMENTATION PAGE

1. REPORT NUMBER: ARO 18414.6-EG	2. GOVT ACCESSION NO.: AD-A146 276 N/A
3. RECIPIENT'S CATALOG NUMBER: N/A	READ INSTRUCTIONS BEFORE COMPLETING FORM
4. TITLE (and Subtitle): EFFECTS OF PRIOR AUSTENITE AND FERRITE GRAIN SIZE ON FRACTURE PROPERTIES OF A PLAIN CARBON STEEL	5. TYPE OF REPORT & PERIOD COVERED: TECHNICAL REPORT
	6. PERFORMING ORG. REPORT NUMBER
7. AUTHOR(s): H. COUQUE, J. DUFFY AND R.J. ASARO	8. CONTRACT OR GRANT NUMBER(s): DAAG29 81-K-0121
9. PERFORMING ORGANIZATION NAME AND ADDRESS: BROWN UNIVERSITY, DIVISION OF ENGINEERING, PROVIDENCE, RI 02912	10. PROGRAM ELEMENT, PROJECT, TASK AREA & WORK UNIT NUMBERS
11. CONTROLLING OFFICE NAME AND ADDRESS: U. S. Army Research Office, Post Office Box 12211, Research Triangle Park, NC 27709	12. REPORT DATE: JULY 1, 1984
	13. NUMBER OF PAGES: 42
14. MONITORING AGENCY NAME & ADDRESS (if different from Controlling Office)	15. SECURITY CLASS. (of this report): Unclassified
	15a. DECLASSIFICATION/DOWNGRADING SCHEDULE

16. DISTRIBUTION STATEMENT (of this Report)

Approved for public release; distribution unlimited.

17. DISTRIBUTION STATEMENT (of the abstract entered in Block 20, if different from Report)

NA

18. SUPPLEMENTARY NOTES

The view, opinions, and/or findings contained in this report are those of the author(s) and should not be construed as an official Department of the Army position, policy, or decision, unless so designated by other documentation.

19. KEY WORDS (Continue on reverse side if necessary and identify by block number)

PRIOR AUSTENITE
FERRITE
FRACTURE
CARBON STEEL

20. ABSTRACT (Continue on reverse side if necessary and identify by block number)

An investigation was conducted into the effects of temperature, loading rate, and various microstructural parameters on the initiation of plane strain fracture of a plain carbon AISI 1020 steel. Ferrite and prior austenite grain sizes were chosen as the principal microstructural features to be investigated. The microstructural variations were accomplished by changing austenitizing temperature and by altering cooling rates during normalization. Fracture toughness tests were conducted using pre-cracked notched round bars loaded in

DD FORM 1 JAN 73 1473 EDITION OF 1 NOV 65 IS OBSOLETE

UNCLASSIFIED
SECURITY CLASSIFICATION OF THIS PAGE (When Data Entered)

tension at two loading rates, viz. $\dot{K}_I = 1.0$ MPA$\sqrt{m}$ s^{-1} and $\dot{K}_I = 2 \times 10^6$ MPA$\sqrt{m}$ s^{-1}. In addition, quasi-static uniaxial tension tests and Charpy impact tests were conducted along with both quasi-static and high rate plasticity tests. The plasticity tests were done in torsion at strain rates of $\dot{\gamma} = 5.0 \times 10^{-4}$ s^{-1} and $\dot{\gamma} = 1.5 \times 10^{3}$ s^{-1}. Testing temperatures covered the range from -150°C to 100°C which encompassed fracture initiation modes involving transgranular cleavage to fully ductile fracture. The results are briefly discussed in terms of simple phenomenological models for fracture.

A-1

Effects of Prior Austenite and Ferrite Grain Size on Fracture Properties of a Plain Carbon Steel

by

H. Couque*, J. Duffy** and R.J. Asaro**

ABSTRACT

An investigation was conducted into the effects of temperature, loading rate, and various microstructural parameters on the initiation of plane strain fracture of a plain carbon AISI 1020 steel. Ferrite and prior austenite grain sizes were chosen as the principal microstructural features to be investigated. The microstructural variations were accomplished by changing austenitizing temperature and by altering cooling rates during normalization. Fracture toughness tests were conducted using pre-cracked notched round bars loaded in tension at two loading rates, viz. $\dot{K}_I = 1.0$ MPa$\sqrt{m}$ s^{-1} and $\dot{K}_I = 2 \times 10^6$ MPa $\sqrt{m}$ s^{-1}. In addition, quasi-static uniaxial tension tests and Charpy impact tests were conducted along with both quasi-static and high rate plasticity tests. The plasticity tests were done in torsion at strain rates of $\dot{\gamma} = 5.0 \times 10^{-4} s^{-1}$ and $\dot{\gamma} = 1.5 \times 10^{3} s^{-1}$. Testing temperatures covered the range from -150°C to 100°C which encompassed fracture initiation modes involving transgranular cleavage to fully ductile fracture. The results are briefly discussed in terms of simple phenomenological models for fracture.

---

* Research Assistant, Division of Engineering, Brown University, Providence, RI, 02912

** Professor, Division of Engineering, Brown Univeristy, Providence, RI, 02912

I. INTRODUCTION

This study is intended to explore the effects of heat treatment and microstructure on plane strain fracture toughness of a pearlitic-ferritic plain carbon steel. Specifically the fracture behavior of an AISI 1020 steel was studied at two loading rates corresponding to quasi-static and high rate loading and over a range of temperatures at which fracture initiation was either by cleavage or fibrous mechanisms or a combination of both. There have indeed been numerous studies over the past 35 to 40 years aimed at similar correlations of heat treatment and microstructure with fracture but few have covered the range of temperature and loading conditions of the present study. Previous work on plain and mild steels, recently reviewed by Gladman et al (1), has relied predominantly on the Charpy impact test, and measurements of the ductile to brittle transition temperature range, to demonstrate and quantify the influence of steel chemistry and microstructure. In the present study quasi-static and dynamic plane strain fracture toughness measurements are employed in order to generate toughness-microstructure correlations which can be analyzed with quantitative micromodelling. There has been, to our knowledge, no other study in which quasi-static and dynamic fracture toughness have been determined over wide temperature ranges in similar steels and in which the microstructure was varied. Indeed there have been very few studies of any type which have attempted to document plane strain fracture toughness at both quasi-static and truly dynamic loading rates, and over a range of temperatures.

However, studies of dynamic fracture in which material effects have been a focus are of increasing interest and are being pursued. Recent work by Curry et al. (2) examined the effects of loading rate on the fracture of a pressure vessel steel with an "as-received" ferritic-pearlitic microstructure. There is a certain phenomenological consistency between their results and those presented here which will be explained below. Other work by Klepaczko and Solecki (3) has examined the influence of loading rate and tempering on the room temperature toughness of a quenched and tempered 5140 H steel. In this work a careful study was made of the effect of tempering, including the use of phenomenological fracture models to relate the measured fracture toughness to the bulk ductilities. A noteworthy trend of the last two studies, which was in fact documented earlier by Costin et al. (4) and Wilson et al. (5) and which was found in the present study, was that at higher

temperatures at which fractures are fully fibrous, fracture toughness is generally greater under high rate loading conditions than under quasi-static loading. At a given temperature (cf. the behavior at 100°C, Fig. 14) increases in K_{Ic} of up to 30 percent are commonly observed when the rate of application of stress intensity is increased from values of order 1.0 MPa$\sqrt{m}$ s^{-1} to 2 x 10^6 MPa$\sqrt{m}$ s^{-1}. This trend is in marked contrast to the behavior observed in the ductile-brittle transition temperature region where dynamic fracture toughnesses are generally lower than those measured under quasi-static loading. There are other studies of the influence of loading rate on high speed fracture which are not reviewed here in the interest of space. However, these studies have not been concerned, as is the present work, with correlations of microstructure, loading rate, and temperature on fracture toughness.

Three microstructures were chosen for the present study, all produced by simple normalization heat treatments. The principal microstructural variations involved prior austenite and ferrite grain size, along with accompanying changes in pearlite volume fraction and colony size. Austenite grain size was varied by changing austenitizing temperature, whereas the ferrite grain size was controlled by the cooling rate from the austenitizing temperature. These three specific microstructures, designated T1, T9 and T7 in what follows, were selected from a much wider series of heat treatments. Our plan was to vary both austenite and ferrite grain size, Table I. This was effected by means of heat treatments that involved rapid cooling (in an air blast) from above 700°C or furnace cooling and that produced microstructures characterized by similar uniaxial tensile properties. The data presented in Section 4 show this was achieved.

In addition to the fracture tests, quasi-static and dynamic plasticity tests were made for the three microstructures over the same temperature range used in the fracture studies, viz. -150° C to 100° C. These allowed correlations between microstructure and yield strength and strain hardening that could be used in analyzing the fracture tests.

The results show a complex dependence of fracture toughness on microstructure whereas the dependence of Charpy toughness was more in accord with a commonly accepted dependence of ductility or toughness on grain size. For the microstructure characterized by the largest combination of prior austenite and ferrite grain size the ductile to brittle transition temperature

range is highest, with little change in either the upper or lower shelf energies. The phenomenology of plane strain fracture toughness, however, has a more complex temperature and loading rate dependence. At temperatures below -50° C, or above 100° C the finer microstructure, characterized by a combination of small prior austenite and ferrite grain sizes, has either larger or nearly equal K_{Ic} values compared with those displayed by the coarsest microstructure. However, in the temperature range between 23° C (room temperature) and 60° C, K_{Ic} was actually larger for the coarsest microstructure. This is an interesting observation which has, in fact, similarities to the room temperature variation in plane strain fracture toughness in ultra high strength quenched and tempered martensitic steels (6-8). This trend, however, did not appear for dynamic toughnesses. The dynamic fracture toughnesses, K_{Id}, were generally lower than the quasi-static toughnesses and the transition to ductile fracture occurred at higher temperatures. At temperatures where plane strain fractures were fibrous, however, the dynamic toughnesses are generally higher than the quasi-static toughnesses for a given microstructure. This is a trend noticed by others, as mentioned above, and is discussed in more detail later.

The plan of this paper is as follows. In Section II a very brief discussion of fracture in plain carbon steels is given which helps put the present study in perspective. In Section III experimental details are given; in particular, the heat treatments are described and the dynamic torsion plasticity tests and stress wave loading fracture initiation methods are described. In Section IV the results are presented and in Section V some discussion and conclusions are given.

II. PERSPECTIVES ON DUCTILE VERSUS BRITTLE FRACTURE IN PLAIN CARBON STEELS.

Plain carbon steels with pearlitic-ferritic microstructures fracture predominantly in two different modes: at low temperatures fracture occurs by transgranular cleavage and at high temperatures by fibrous mechanisms involving void growth and coalescence. These modes exist whether specimens are loaded, or strained, at very high rates (in particular at strain rates in the range used in the present study of $10^2 s^{-1}$ to $10^3 s^{-1}$) or at quasi-static rates in the range $10^{-4} s^{-1}$ to $10^{-3} s^{-1}$. In the temperature range between -40° C to 100° C fracture modes undergo the well known transition from cleavage to fibrous which is accompanied by a large increase in toughness.

The transition can occur over a broad or very narrow temperature interval and the details of this, along with the specific temperatures at which the transition takes place depend sensitively on alloy chemistry, heat treatment and microstructure. In general, the temperature range over which cleavage predominates is raised to higher temperatures with increases in loading or strain rate, or with changes in microstructural features such as increases in grain size or the density and thickness of the grain boundary carbides which initiate cleavage.

Correlations of microstructure and impact fracture toughnesses (mainly Charpy energy) have been the focus of recent studies on fully pearlitic steels (9,10) and have been widely explored for low carbon, or mild, steels. For plain carbon steels with pearlitic-ferritic microstructures there have been fewer studies; the present work is meant to provide such a study.

In pearlite-free steels the studies of Bruckner (11), Allen et al. (12), Josefsson (13), Petch (14), and Mintz et al. (15), among others, have shown that cleavage fracture and the ductile to brittle transition are strongly influenced by ferrite grain size, by carbon content, and by the density and size, i.e., thickness, of iron carbides. These early studies (11-13), however, also emphasized the importance of the properties of the ferrite itself. This is noteworthy since more recent discussions of cleavage have tended to focus more on the role of carbides in initiating cracks and have not attempted to describe why, or how, microcracks propagate in a brittle fashion rather than blunt out into voids. Indeed, the abstract of Allen et al. (12) states, with reference to the increase in transition temperature, that "This is associated with the production of cracks in the carbide, which are considered to initiate cleavage of the ferrite at a temperature at which it should be ductile in the absence of the carbide films". This early work clearly recognized that ferrite itself is a ductile phase at temperatures at which mild steels cleave. What remains to be learned, however, is whether it is sufficient to have static microcracks, or microcracks introduced dynamically when carbides undergo brittle fracture, to trigger a "brittle like" cleavage in a ductile ferrite. In any event, it seems that the properties of the ferrite, e.g., strength, strain rate sensitivity, and tendencies toward twinning versus slip determine how the tip of a fast moving microcrack will behave, i.e., whether it will blunt or continue to run with a sharp front.

Bruckner (11) provided convincing metallographic evidence in a number of hypoeutectoid steels that cleavage cracks initiate at grain boundary carbides and propagate through ferrite grains at temperatures within and below the transition range. He also showed that such cracks initiate within pearlite colonies. Pearlite colonies, oriented so that the carbide lamella are alligned within 45° to the direction of maximum principal tensile stress, were observed to crack preferentially. At higher temperatures cracks also initiate but rather than propagating as cleavage cracks they blunt out to form voids which grow and coalesce by plastic flow to cause fibrous fracture. Bruckner's experiments were performed on steels with carbon contents in the range 0.19-0.27 wt percent and on Armco iron. The steels were either killed, semikilled or rimmed. He emphasized that his killed steels were much more ductile than either the semikilled or rimmed steels; in particular, cracks that initiated at carbides or within pearlite colonies in the killed steels tended to blunt into voids at temperatures where the less effectively deoxidized steels cleaved. He argued that the tendency for cleavage correlated with the degree of mechanical twinning and thus with a reduced ductility of the ferrite matrix itself. There are several other obvious metallurgical factors which may have indeed contributed to Bruckner's observations, e.g., grain size differences among the steels he studied and differences in carbon concentration (the rimmed and semikilled steels had slightly larger carbon contents than the killed steels). Nonetheless, his results suggest that in comparable microstructures with similar crack initiating features, the tendency for microcracks to propagate as cleavage cracks rather than blunt in a ductile fashion is strongly influenced by the constitutive properties of the ferrite.

Additional correlations between the onset of cleavage and the ductile-brittle transition were made by Allen et al. (12) on a series of low carbon Fe-C and Fe-C-Mn alloys which, for the most part, were pearlite free. Their results strongly confirm the relationship between the appearance of carbides and low toughness cleavage fractures. In making this correlation a good deal of attention was paid to the influence of cooling rate from the austenite during heat treatment: in general, it was found that increased cooling rates (from furnace cooling to water quenching) reduces the transition temperatures thus extending the ductile range. In addition the temperature interval over which the transition occurred was much less for the rapidly cooled steels. This effect of cooling rate was attributed to the higher retention of carbon

in solution with the faster cooling and thus a lower density, and average thickness, of grain boundary carbides. They also included a study of the influence of manganese additions on ductile versus brittle behavior and found that, except for alloys containing 2 wt percent Mn and water quenched, the general effect is to lower the transition temperature and to increase ductility. In large part this was attributed to manganese inhibiting carbide formation but they also pointed out that such alloying additions also affect constitutive properties of the ferrite, viz. strength and strain rate sensitivity.

In a later study, Burns and Judge (16) explored some effects of heat treatment on plain carbon steels with fixed carbon content. They varied austenitizing temperature and cooling rate for the purpose of varying prior austenite and ferrite grain size, as well as pearlite colony size. Their findings are consistent with those reported earlier by Allen et al. (12) and Bruckner (11) in that the transition temperature range generally tended to shift to lower temperatures as the cooling rate increased, or accordingly, as the sizes of the above-mentioned microstructural features decreased. Indeed, the Burns and Judge (16) results are most naturally interpreted as a comparative study of the relative effects of prior austenite grain size versus ferrite and pearlite grain sizes. Their results indicated that increasing ferrite grain size tended to shift the ductile-brittle transition to higher temperatures. However, the effect of austenitizing at higher temperatures, and thus producing larger prior austenite grain sizes, was just as large and in fact the largest increases in transition temperature were observed when the austenitizing temperature was increased from 860 C to 1150 C. It is difficult to separate the relative effects of grain size and carbide precipitation in these studies just as it is difficult to separate them in the studies on low carbon alloys by Bruckner (11), Allen et al. (12) and Josefsson (13). However, there is additional reason to suspect that prior austenite grain size itself is a controlling microstructural feature. For example, Bernstein and co-workers (9,10) have provided convincing evidence that cleavage in fully pearlitic steels is controlled by the size scale in the ferritic grain structure over which a continuous crystallographic cleavage plane orientation is maintained. They argue that this scale is inherited from the austenite grain structure and monotonically scales with the austenite grain size.

Mintz et al. (15) separated the various effects of microstructure by

carrying out multilinear regression analyses of ductile-brittle transition temperatures. Their analysis accounts for grain size and pearlite volume fraction along with effects of chemistry: in particular the beneficial effects of manganese were also described. Their analyses are novel among others of this sort, however, in that they included a description of the effect of carbide thickness. In this way their analysis suggests that large grain size and carbide thickness each play roles and thus represent distinct influnces on promoting cleavage. The beneficial effects of manganese, which arise mostly through a refinement in carbide thickness, were also described by the analysis of Mintz et al. Additional effects of manganese were noted, however, that were attributed tentatively to grain boundary segregation effects.

In summary, studies, such as those briefly described here, have shown that fracture in ferrite steels is controlled by microstructural features such as grain size and carbide morphology. In particular, the transition to transgranular cleavage from fibrous fracture at lower temperatures depends sensitively on both ferrite and prior austenite grain size and thus on the thermal histories imposed during heat treatment. It must be noted, though, that changes in carbide morphology are generally coupled to those in grain size; for example, in lower carbon steels it is especially important to note that slower cooling rates during normalizing lead to both coarser carbides and larger ferrite grains which makes separation of their effects difficult. This is an important consideration in interpreting Petch's (14) correlations of fracture strength and grain size since the grain size variations he reports on were achieved by controlling cooling rates. In addition, it also appears that there are important effects of alloying and heat treatment on the constitutive properties of the ferrite itself--effects of manganese additions on strength, strain rate sensitivity, and ductility have been noted by Allen et al. (12) and Josefsson (13). In the present study we have chosen to focus on variations in austenite and ferrite grain size which in plain carbon steels have been shown to play a dominant role.

The mechanistics of fracture in low carbon and plain carbon steels was also made clear in these early studies carried out between 1950-1955. A summary discussion of mechanisms and modelling of cleavage was given by Cottrell (17) in 1958. The basic idea is that when the ferrite matrix in the bulk of a smooth tensile specimen or at the tip of a crack is plastically strained in the vicinity of a carbide plate or pearlite colony, the

concentrated stresses in the carbide cause it to crack in a brittle fashion. Brittle fracture of a carbide introduces a nearly atomically sharp crack into the adjacent ferrite grain. The question then is whether the crack blunts by plastic flow in the ferrite, a process that would depend on the constitutive properties of the ferrite and on the mechanisms of initiation of plastic flow at a crack tip, or whether it propagates by crystallographic cleavage. Allen et al. (12) focus on the fact that ferrite itself is inheretly ductile at temperatures at which mild steels cleave and, although they did not carry through a detailed analysis of the mechanics of crack tip behavior, they pointed out how the field of a crack tip, with high triaxial constraints, might inhibit local ductility and allow cleavage. What has not been recognized in the formulation of models for cleavage used to discuss ductile-versus-brittle response is that the microcracks that initiate at carbides are initiated dynamically, and thus attempt their penetration into ferrite at very high speed. Thus what is needed to explain the onset of cleavage is an analysis of the response of a dynamically introduced crack in ferrite. Constitutive properties such as strength (which would determine the "far-field" stresses driving such a microcrack), and strain rate sensitivity (which would influence the response of the ferrite and its ability to plastically respond fast enough to blunt the moving crack), will both influence the material's response to the moving crack tip. In fact, even some of the commonly observed effects of loading rate would enter such a model, in part through the strain rate sensitivity since at higher loading rates the prevailing stresses would be larger. Such refined models are not yet available and instead current models are based on the phenomenological notion (which is inherently static and does not include time or rate effects) that cleavage occurs once a critical stress is reached over those regions which contain crack initiating sites. The present discussion is concluded with a very brief statement of these models to the extent they are relevant to the present work.

The paper by Cottrell (17) contains a clear statement of the prevailing notion that cleavage occurs when a critical fracture stress is reached which is sufficient to initiate and drive microcracks. If this stress is lower than the bulk yield stress then the material cleaves; if it is larger, yielding occurs and the material is ductile. Cracks initiate by plasticity and models proposed include the impingement of slip bands on carbides (18) and fiber

loading of cementite lamella in pearlite (19). In fact, at temperatures in the transition regime fracture strains are appreciable in plain carbon steels and it seems sensible to argue that cleavage initiates at a critical strain. Cottrell's analysis is not repeated here but it should be noted that his model emphasized two features of the process. In the first place, he noted that the fracture stress had to be sufficient to drive cracks after their nucleation and at higher temperatures this accounts for the fact that it is larger than the yield stress. In the second place, the process of nucleation and growth requires that this stress be achieved over a distance of at least one ferrite grain diameter--in the case where fractures initiate at carbides this means that the fracture stress must also be achieved over distances which include carbides. In analyzing our own results later on we make use of a simple and commonly used phenomenological fracture criterion based on Cottrell's discussion, viz. that for fracture to occur a critical strain must be achieved over a critical distance. The model is applied only at temperatures within the transition where the fracture mode is mixed cleavage and fibrous.

III. EXPERIMENTAL DETAILS

III.1 Material and Microstructures

The material used was an AISI 1020 steel received in the form of hot rolled rods, 2.54 cm in diameter. Since the fracture specimens (described in the next section) were themselves long rods of lengths between 72 and 117 cm a tube furnace was used for heat treating. Different prior austenite grain sizes were obtained by varying the austenitizing temperature in the range 860°C to 1000°C. Furnace cooling, air cooling and air blast cooling were used in order to vary the ferrite grain size. Observations of the ferritic-pearlitic microstructure were made normal to the rolling direction and are reported in Table I for the three microstructures we settled on for the present study. These observations were made by mechanical polishing and etching with 3% nital solution for 10 to 12 seconds. For measurement of the prior austenite grain size a second set of specimens was austenitized and quenched in a continuously stirred brine solution. The specimens were then mechanically polished and etched for 30 seconds in the following solution: 1 mg of sodium tridecylbenzene sulfate in 100 ml of distilled water heated at 70°C and then mixed in dry picric acid until saturation. Microstructural measurements were repeated on at least two specimens with micrographs taken

from several locations on each specimen. In addition, microstructures were examined on most test specimens to confirm they conformed to the intended grain sizes.

As mentioned earlier three separate microstructures were employed in this investigation and their characteristics are listed in Table I along with a statement of the heat treatment detail. These three microstructures were chosen from a group of some twenty microstructures because they span a wide range of grain sizes and yet have similar uniaxial tensile strengths and strain hardening characteristics. The finest microstructure, designated T1, is characterized by the finest ferrite and prior austenite grain sizes which are shown in Figs. 1a and 1b; the coarsest microstructure, T7, has the largest ferrite and prior austenite grain sizes which are shown in Figs. 2a and 2b. Each of the heat-treatments was further characterized by hardness tests, Charpy impact tests and by routine tensile tests at room temperature on standard size specimens. The results are presented in Table II. The tensile stress-strain curves are shown in Fig. 3, which shows that although there is a larger yield drop for microstructure T7 and thus a smaller lower yield point the flow stresses are quite comparable at strains beyond about 3 percent.

III-2 Description of the Fracture Initiation Experiment

The dynamic fracture initiation test employed in this study was first introduced by Costin et al. (20), subsequently used in other experiments (4,5), and further modified in the present investigation as outlined below. Essentially, the test consists in loading to failure a pre-cracked notched round bar of 2.54 cm diameter by means of a rapidly rising tensile pulse resulting from an explosive detonation initiated at one end of the bar, see Fig. 4, to produce a loading rate of $\dot{K}_I = 2 \times 10^6$ MPa $\sqrt{m}$ s^{-1}. A circumferentially uniform fatigue crack is grown in from the root of the notch in a rotating bending apparatus, Figs. 5 and 6. A photograph of a typical fracture surface is shown in Fig. 7. The explosive charge is placed against a mass bolted to the end of the bar, so that when it is detonated the mass pulls away from the bar, thus initiating the tensile pulse. For tests at low or elevated temperatures an environmental chamber encloses the notched section of the bar. For the present tests, the charge was detonated inside a vacuum chamber in order to avoid possible damage to the instrumentation. The tensile pulse is monitored by a set of strain gages as it travels toward the pre-

cracked section of the bar, since it is essential that its amplitude be large enough so fracture occurs on the rising portion of the pulse. A second set of gages monitors the pulse transmitted through the pre-cracked section, thus providing a measure of average stress at the fracture site in accordance with the principle behind Kolsky's split-Hopkinson bar (21). The instant of fracture initiation is determined from observations of the transmitted and reflected pulses. Crack opening displacement is measured optically by an adaptation of the moire technique in which a glass slide is mounted to span the notch in the bar but cemented only to one side of the notch. A grid of 33 lines/mm is deposited photographically on the bar and a matching grid on the glass slide, so that as the crack opens the two grids slide past each other. Their relative displacement is determined from changes in the interference pattern using a photodiode. Thus the instrumentation provides measures of average stress at the fracture site and of crack opening displacement, each as a function of time, that are used for calculating a critical stress intensity factor K_{Ic}, or J_{Ic} when the metal is more ductile. The method of calculation and an estimate of its accuracy are presented in the next paragraph.

For a nominally brittle material the parameter of interest is K_{Ic}, the plane strain fracture toughness. According to Tada et al. (22)

$$K_I = \frac{P}{\pi R^2} \sqrt{\pi R}\ F\ (2R/D) \qquad (1)$$

where R is the radius of the unfractured ligament, P is the applied load, D is the diameter of the bar, and F(2R/D) is a size function equal to about 0.48 in the present experiments. The load P used in calculating K_{Ic} from Equation (1) is determined from the load-displacement curve in accordance with ASTM standards by using the 5% slope offset procedure. In order to apply linear fracture mechanics concepts, the size of the crack tip plastic zone must be small compared to the nominal dimensions of the specimen. As a criterion of a valid K_{Ic} test

$$R \geq 2.5(K_{Ic}/\sigma_y)^2 \qquad (2)$$

is used, where σ_y is the flow stress of the material determined at a strain rate comparable to the strain rate achieved near the crack tip region during the fracture test. The required dynamic flow stress for each temper was

determined using a torsional Kolsky bar as described in the next section. The specimens used for this purpose were cut after performing the fracture tests from a portion of the bar near the fracture site, Fig. 6.

When testing more ductile materials, the specimen size is inadequate to contain the plastic zone within the limit imposed by Equation (2). In these cases, a J-integral approach is adopted. Paris (23) has suggested that a possible criterion for a valid J_{Ic} test is

$$R \geq 50\ J_{Ic}/\sigma_y \tag{3}$$

and this criterion was used in determining the validity of present results. Rice et al. (24) have shown that the value of J for a notched round bar may be determined from a load-displacement curve according to

$$J = \frac{1}{2\pi R^2}\left(3\int_0^{\delta} P d\delta_c - P\delta_c\right) \tag{4}$$

where δ_c is the load-point displacement due to the presence of the crack. For present purposes, use of the notch opening displacement at the bar surface was taken for the load-point displacement. The accuracy of this approximation was studied by Nakamura et al. (25) in a recent elastic-plastic analysis of the dynamically loaded circumferentially notched round bar. This analysis, which employs the finite element method, provides a critique of the present experimental method and of the interpretation of results in the case of more ductile materials. In their analysis, Nakamura et al. modelled the experimental conditions by taking the same geometry as in the experiment and by taking the experimental stress-strain curve for AISI 1020 hot-rolled steel deforming at a strain rate of $10^3 s^{-1}$ in shear. A time-dependent tensile load was applied at one end of the bar to simulate the incident loading pulse used in the experiment. An integral expression was then used to calculate the dynamic energy release rate for the axisymmetric bar, taking inertia into account. This calculation of the J-integral shows that the method of evaluating J in the experiment, i.e., by means of equation (4), underestimates its value. The error involved depends upon the ratio 2R/D of unfractured ligament to bar diameter. In experiments we performed prior to the present investigation, we did not have the benefit of this analysis and 2R/D was about 0.4. The resulting calculated value of J, according to Nakamura et al., was

then about 22% too low in the nominally elastic range, gradually going to about 12% too low for a fully plastic section. However, as a result of this finite element investigation, we have modified the depth of the crack, so that in all present experiments 2R/D is about 0.3. This reduces somewhat the error in J: 15% for the nominally elastic domain going to 8% for fully plastic. The error in the equivalent value of K_I thus goes from about 7% to 4%, and is nearer the latter value when critical conditions are reached. The finite element analysis also shows that the location of the strain gages on the bar at a distance of one diameter from the crack provides an accurate measure of the transmitted load. Furthermore, the analysis reveals that Equation (4), should be based on the load transmitted across the ligament and on the notch opening displacement. This was indeed the interpretation taken in (4,5,20). In summary then, the finite element analysis shows that this fracture initiation experiment can provide an accurate value of J_I (or K_I) during dynamic fracture initiation, if the notch in the bar is made sufficiently deep.

The static fracture initiation tests were performed with a precracked notched round bar having the same geometry as the specimens used in the dynamic tests and subjected to the same heat-treatments. Tension to fracture was supplied by a 120,000 pound capacity Riehle universal testing machine, equipped with a load cell; an environmental chamber was used for tests at low temperatures, Fig. 8. In the static tests, the notch opening displacement was measured optically by employing an MTI photonic sensor. As shown in Fig. 8, the instant at which fracture initiated was determined by a measurement of electrical resistivity. A DC current was furnished by a 6 volt power supply connected to the bar at two points 10 cm to either side of the crack. The resistivity between these two points increases linearly with increasing load as long as the crack does not extend; a departure from linearity provides the value of the load and hence of the instant of fracture initiation.

III-3 Dynamic Plasticity Tests

Static and dynamic stress-strain curves for these steels are needed to characterize fully the material and, in particular, to provide a value of dynamic flow stress needed for use in Equations (2,3). Specimens were tested in the torsional Kolsky bar (split-Hopkinson bar) first described by Duffy et al. (26) and later modified by Costin et al. (27). A schematic diagram of the

experiment is shown in Fig. 9. The specimen, machined from the fracture specimen after testing, consists of a short thin-walled tube mounted in the bar by means of a pair of flanges, Fig. 9. To obtain a dynamic stress-strain curve, a torque is stored between pulley A and clamp B. Upon sudden release of the clamp by the fracture of a breaker piece, a torsional loading pulse, with an amplitude half as great as that stored, propagates down the bar toward the specimen, while an unloading pulse of equal magnitude propagates from the clamp toward pulley A. Upon reaching the specimen, part of the pulse is transmitted and part is reflected. Strain gages are mounted on the bar to either side of the specimen and, following Kolsky's original technique (21), it can be shown that the transmitted pulse gives a measure of shear stress in the specimen as a function of time while the reflectd pulse provides a measure of shear strain rate. Calibration of the gage outputs is described in the references. The stress-strain curve is obtained by integrating the reflected pulse to give shear strain and eliminating time between the stress-time and strain-time signals. By this means a stress-strain curve is obtained at a strain rate of about $10^3 s^{-1}$. The same apparatus is employed to obtain a static stress-strain curve. For this purpose the pulley at D is rotated by a slowly turning electric motor drive, while the variable speed drive while the clamp is fixed. A pair of direct current differential transformers measures the rotation of the bar to either side of the specimen, while strain gages on the bar provide a measure of torque. Thus a static stress-strain curve is established in shear at a strain rate of about $5 \times 10^{-4} s^{-1}$ using specimens of identical geometry with the dynamic specimens. Tests at elevated temperature were performed by enclosing the specimen in a radiant heating clam shell furnace, while the temperature was measured by a thermocouple attached to the flange of the specimen. An environmental chamber with a controlled flow of nitrogen gas from a liquid nitrogen bottle was used to attain the cold temperatures.

IV. RESULTS

IV.1 Plasticity

Figs. 10-12 show results of the torsion tests for the two extreme microstructures T1 and T7 over the temperature range -150°C to 100°C. Fig. 10 shows a comparison of the shear stress-shear strain curves obtained at the quasi-static strain rate at three temperatures bracketing room temperature.

At both 60°C and 23°C (room temperature) the stress-strain behavior is quite similar for the microstructures T1 and T7 with the finer microstructure displaying slightly higher strength. At -60°C the strength level is substantially higher than at the higher temperatures and, what is perhaps unexpected, the coarser microstructure T7 is stronger. In all cases, though, the strain hardening characteristics are similar and the microstructures all display significant ductilities. These data were reduced using a simple power law

$$\tau/\tau_y = (\gamma/\gamma_y)^n \qquad (5)$$

where τ_y and γ_y represent, respectively, the values of the initial yield stress and strain, and where n is the hardening exponent. As may be seen in Table III, initial yield stress values in shear are somewhat lower for the coarser microstructures but their strain hardening exponents somewhat greater. Since they have opposite effects on the flow stress level they combine to produce quite similar stress-strain behavior.

Figs. 11 and 12 show both dynamic and quasi-static torsion results over the larger temperature range -150°C to 100°C. At each temperature a significant increase in flow stress is seen to accompany the increase in strain rate from $\dot{\gamma} = 5 \times 10^{-4} s^{-1}$ to $\dot{\gamma} = 1.5 \times 10^{3} s^{-1}$. For example, and for later reference, we note that at 100°C there is an approximately 40 percent increase in flow stress at the higher strain rate. On the other hand, the differences in flow stress between the two microstructures T1 and T7 at the high strain rate at a given temperature are small as is the case at the quasi-static strain rate. At a temperature of 23°C or higher the finer microstructure has a slightly larger flow stress. However, at lower temperatures, e.g, -150°C in Figs. 11 and 12, the coarser microstructures have the larger flow stress. This trend is again similar to that observed at quasi-static strain rates.

IV.2 Charpy Impact Energy

Fig. 13 shows the results of a series of Charpy impact tests conducted over the temperature range -60°C to 100°C. The lower shelf and upper shelf impact energies do not differ substantially between the two microstructures although the upper shelf energy for the finer microstructure is slightly greater. The transition from cleavage to ductile fracture occurs at higher

temperatures for the coarse microstructure which is consistent with the general trends found in the literature (1,15,28).

IV.3 Plane Strain Fracture Toughness

Fig. 14 shows a nearly complete set of fracture toughness values for the coarse T7 and fine T1 microstructures obtained over the temperature range -150°C to 100°C. Overall the trends in K_{Ic} and K_{Id} are similar to those observed for the Charpy impact energies. For the dynamic fracture toughnesses there is an apparent lower shelf toughness that extends up to about room temperature, i.e. 23°C. Above 23°C the dynamic fracture toughness, K_{Id} rises rapidly to an apparent upper shelf that is reached at about 100°C. The fine microstructure, T1, is always tougher than the coarse microstructure, T7, while the loading rate is at this high rate; however, at 100°C the difference between the two microstructures is quite modest. For the quasi-static fracture toughnesses there is, on the other hand, a rather different, and intriguing, behavior in the temperature range -60°C to 60°C. In this temperature range the curves plotting the K_{Ic} values for the fine and coarse microstructures cross each other twice with the values associated with the coarse microstructure being higher in the temperature range including 23°C to 60°C. It may be noted that in this temperature range fractures are of a mixed cleavage-fibrous type and in what follows we use a critical fracture strain criterion to attempt an explanation of the effect.

Another interesting feature of the fracture toughness values shown in Fig. 14 is that, when the fractures are fully fibrous, the dynamic fracture toughnesses are larger than those measured quasi-statically. At a test temperature of 100°C, for example, the plane strain fractures of the fine microstructure are fully fibrous for both quasi-static and dynamic loading. At this temperature the dynamic fracture toughness is about 35 percent larger than when measured quasi-statically. This is a trend which is commonly observed (1,3) and may well be attributed in large part to the higher flow stresses that prevail at the higher rate.

In Fig. 14 the fracture mode is indicated at each temperature in a qualitative way by the symbols "C" for cleavage, "F" for fibrous and by "CF" for a mixed mode of cleavage and fibrous fracture. In Fig. 15 the relative proportions of cleavage and fibrous fracture are shown for each microstructure. There is a rather general correlation between the increase in

fibrous fracture and increases in either K_{Ic} or K_{Id} but the correlation is by no means a close one. For example, in the temperature range that includes the interval between 23°C and 60°C the percentage of fibrous fracture is some 20 to 30 percent larger for the finest microstructure than for the coarsest microstructure for quasi-static fractures. In this same temperature range, however, the fracture toughnesses were found to be higher for the coarse microstructure. In addition at 100°C for the dynamic fractures the coarsest microstructure displayed fractures that were barely 10 percent fibrous whereas in the fine microstructure fractures were completely fibrous. Despite this large difference in fracture mode the dynamic fracture toughnesses for both microstructures are seen in Fig. 14 to be similar. At the same time it should be noted that for the coarsest microstructure the dynamic fracture toughness is larger than the quasi-static toughness. This does not, however, fit the general trend noted earlier for dynamic versus quasi-static fracture toughnesses since in this case the fracture mode is fully fibrous only for quasi-static loading.

V. DISCUSSION

A full discussion of the results presented above is not possible in this preliminary report since a full analysis requires completion of the microstructural studies currently underway. These studies include further quantification of the fracture surface topographies along with detailed studies of the micromechanics of fracture. The latter studies will include observations of cleavage initiation as well as microvoid initiation and growth. Progress can be made, however, with a tentative model approach and thus this discussion, although preliminary, should prove useful for a later analysis of the more complete set of data.

A useful starting point for interpreting the fracture results is the model proposed by Rice and Johnson (29) for ductile fracture beneath a sharp crack. The model rests on the idea that fracture occurs when critical strains are achieved over critical distances, i.e., over size scales in the microstructure that contain the features which are responsible for initiating fracture. Rice and Johnson proposed the model originally to account for ductile crack extension via void growth and coalescence with a blunting crack tip. However, with the earlier discussion concerning slip induced cleavage in mind, we will attempt to use their basic idea to model fractures occurring in

the ductile brittle transition temperature regime. In particular the model idea is used to provide an explanation of the variations in quasi-static fracture toughness in the temperature range 23°C to 60°C. To implement the fracture model McMeeking's (30) numerical solutions for blunting crack tips is used.

McMeeking's results provide relationships between the crack tip opening displacement δ_t and the value of the applied loading, measured as the value of the applied J integral. The constitutive law used in the calculations was J_2 flow theory with power law strain hardening. McMeeking carried out specific calculations for material models for which the strain hardening index n=0.2 and the ratio of yield strength to elastic modulus $\sigma_y/E = 1/300$: in this case δ_t is related to J and σ_y via

$$\delta_t = 0.27\ J_{Ic}/\sigma_Y \tag{6}$$

Now for small scale yielding K_I is related to J through the relation (2) and thus if such conditions apply the above relation for δ_t becomes

$$\delta_t = 0.27\ (1 - \nu^2)\ K_I^2/\sigma_y\ E \tag{7}$$

which then gives, once $\delta_t = \delta_t^*$ is substituted,

$$K_{Ic} = \sqrt{\sigma_y\ E\ \delta_t^*/(0.27)\ (1 - \nu^2)} \tag{8}$$

McMeeking's results indicate that the plastic strain, defined as an effective strain, monotonically decreases with the parameter r/δ_t, where r is the radial distance from the crack tip. There is a range of such curves corresponding to a different value of θ, the angle a ray emanating from the crack tip to the field point makes with the crack line. An interesting feature of all these curves is that they rise very steeply for plastic strains exceeding 0.20 or so, corresponding to a value of $r/\delta_t \approx 0.5$. Since the ductilities of all the microstructures studied here lie well above 0.20, this implies that to invoke the ductile fracture criterion of a critical strain over a critical distance the plastic strain curve would be entered at a value of $(r/\delta_t) \approx 0.5$. Now suppose we rewrite Equation (8) as

$$K_{Ic} = \sqrt{\sigma_Y E r / (0.27)(1-\nu^2)(r^*/\delta_t^*)} \quad (9)$$

where r* is the critical microstructural distance over which strains in excess of 0.20 must be achieved. By the argument given above (r^*/δ_t^*) may be taken as approximately equal to 0.5 and when this is substituted into Equation (9) the result is

$$K_{Ic} \approx \sqrt{7.4\ \sigma_y E \sigma^*/(1-\nu^2)} \quad (10)$$

The result represented by Equation (9) is noteworthy in several respects. In the first place, so long as the fracture process zone is confined to a region not more than, say, twice δ_t (i.e., within the finite strain region at the crack tip) the dependence of K_{Ic} on ductility will be slight. Secondly, it should be noted that for similar microstructures, i.e., with comparable values of r*, $K_{Ic} \alpha \sqrt{\sigma_y}$ which suggests that K_{Ic} should increase with strength.

Table IV shows some computed values of K_{Ic}, based on Equation (10), compared with measured values obtained in the quasi-static notched bar test. The calculations are based on taking r* equal to the prior austenite grain size. What is encouraging about these calculations is the reasonable scaling of the predicted K_{Ic} values with the measured toughness values. In general, as the microstructure coarsens and r* increases, K_{Ic} increases roughly as the square root of grain size. In this temperature range the fracture mode is mixed fibrous and cleavage and thus it is reasonable to speculate that the spacings of those microstructural features responsible for cleavage scale with austenite grain size. It must be noted, however, that outside the temperature range 23°C to 60°C the model outlined above actually predicts trends opposite to what is observed. At temperatures much below room temperature (certainly at -60°C) or above 60°C the finer microstructure, T1 , is tougher. The explanation of this requires additional data and much more microstructural study but some tentative ideas can be advanced now which provide a basis for further analysis.

At higher temperatures quasi-static fractures tend to be nearly fully fibrous and thus require the accumulation of plastic strain large enough to initiate, grow, and coalesce voids. If this very ductile process occurs in about the same way in both microstructures--which has yet to be determined by metallographic analysis--the expectation from Equation (10) is that K_{Ic} would scale as $\sqrt{\sigma_y}$. Since the quasi-static yield strengths for both the coarsest and finest microstructures are nearly equal, with the finest microstructure being slightly stronger, this is consistent with the fact that K_{Ic} is only

slightly larger for the fine microstructure at 100°C. On the other hand, for the fine microstructure the dynamic yield strength is approximately 40 percent larger than the quasi-static strength, which suggests that the dynamic fracture toughness should be about 20 percent larger. The actual ratio of dynamic to quasi-static fracture toughness for the fine microstructure is about 1.3. These favorable correlations suggest that a more rigorous modelling of the ductile rupture process at both quasi-static and high rates which accounts for void growth could very well provide an accurate description of the fracture process.

Acknowledgements

The research support of the Army Research Office under Grant No. DAAG29 81-K-0121 and of the NSF Materials Research Laboratory at Brown is gratefully acknowledged.

REFERENCES

1. Gladman, T., McIvor, I.D., and Pickering, F.B., J. Iron Steel Inst. 210, 916 (1972).
2. Curry, D.A., Milne, I. and Gates, R.S., Mat. Sci. Eng., 63, 101 (1984).
3. Klepaczko, J.R. and Solecki, A., Metall. Trans., 15A, 901 (1984).
4. Costin, L.S. and Duffy, J., Trans. of ASME, J. Eng. Mat. Tech., 101, 258 (1979).
5. Wilson, M.L., Hawley, R.H. and Duffy, J., Eng. Frac. Mech., 13, 371 (1980).
6. Parker, E.R. and Zackay, V.F., Eng'g. Fract. Mech, 7, 371 (1975).
7. Ritchie, R.O., Francis, B. and Server, W. L., Metall. Trans. 7A, 831 (1976).
8. Lee, S., Majno, L. and Asaro, R.J., Brown University Technical Report DOE No. 96 (1983).
9. Hyzak, J.M. and Bernstein, I.M., Metall. Trans., 7A, 1217 (1976).
10. Park, Y.J. and Bernstein, I.M., Metall. Trans., 10A, 1653 (1979).
11. Bruckner, W.H., Supplement Weld. J., 467s (1950).
12. Allen, N.P., Rees, W.P., Hopkins, B.E. and Tipler, H.R., J. Iron Steel Inst., 174, 108 (1953).
13. Joseffson, A., J. Metals, 6, 652 (1954).
14. Petch, N.J., J. Iron Steel Inst., 174, 25 (1953).
15. Mintz, B., Morrison, W.B. and Jones, A., Met. Tech., 6, 252 (1979).
16. Burns, G. and Judge, C., J. Iron Steel Inst., 182, 292 (1956).
17. Cottrell, A.H., Trans. AIME, 212, 192 (1958).
18. Smith, E., Acta Metall., 14, 991 (1966).
19. Lindley, T.C., Oates, G. and Richards, C.E., Acta Metall., 18, 1127 (1970).
20. Costin, L.S., Duffy, J. and Freund, L.B., ASTM STP 627, 301 (1977).
21. Kolsky, H., Proc. Phys. Soc. London, 62-B, 676 (1949).
22. Tada, H., Paris, P.C. and Irwin, G.R. in The Stress Analysis of Cracks Handbook, Del. Research Corp., Hellertown, Pennsylvania, (1973).
23. Paris, P.D., in written discussion to Begley, J.A., Landes, J.D., ASTM STP 514, 1 (1972).
24. Rice, J.R., Paris, P.C. and Merkle, J.C., ASTM STP 536, 231 (1973).
25. Nakamura, T., Shih, C.F. and Freund, L.B., Brown University Technical

Report MRL E-152, (1984).

26. Duffy, J., Campbell, J.D. and Hawley, R.H., J. Appl. Mech., 38, 83 (1971).
27. Costin, L.S., Crisman, E.E., Hawley, R.H. and Duffy, J., Mechanical Properties at High Rates of Strain, Ed: J. Harding, 90 (1979).
28. Gross, J.H. and Stout, R.D., Supplement Weld. J., 117s (1955).
29. Rice, J.R. and Johnson, M.A., Inelastic Behavior of Solids, Ed: M.F. Kanninen et al, McGraw-Hill, 641 (1970).
30. McMeeking, R.M., J. Mech. Phy. Solids, 25, 357 (1977).

Table I Description of heat treatments and resulting microstructural characteristics.

Heat Treatment Number	Heat Treatment		Grain Size			Volume Fraction of	
	Austenitizing Temperature, One Hour	Cooling Process	Prior Austenite $L_{3\gamma}$ [μm]	Ferrite $L_{3\alpha}$ [μm]	Pearlite L_{3p} [μm]	Ferrite (%)	Pearlite (%)
T1	860°C	Airblast cooled to room temperature	25.6	13.7	5.6	86.7	13.3
T9	860°C	Furnace cooled to 710°C, then air cooled to room temperature	25.6	22.2	10.1	86.0	14.0
T7	1000°C	Airblast cooled to room temperature	65.2	24.4	8.0	83.5	16.5

Table II Results of Charpy, tensile and hardness tests at 23°C.

HEAT TREATMENT	CHARPY TEST RESULTS		TENSILE TEST RESULTS						HARDNESS
	CHARPY ENERGY [Joules]	FIBROUS FRACTURE [%]	YIELD STRESS evaluated at ε=.002 [MPA]	SLOPE OF THE ENGINEERING STRESS STRAIN CURVE MPA ε=.04	ε=.10	ε=.15	TRUE STRESS AT FRACTURE SITE [MPA]	REDUCTION IN AREA [%]	ROCKWELL [A Scale]
T1	174	95	280	1930	620	260	880	67	44.8
T9	89	59	260	2240	380	140	810	64	44.3
T7	75	58	220	2120	450	150	880	67	42.7

Table III Results of quasi-static torsion tests at 23°C and 60°C

TESTING TEMPERATURE	HEAT TREATMENT	Number of Tests	YIELD STRESS at γ=0.001 MPA	HARDENING EXPONENT n $\gamma_y<\gamma<.35$
23°C	T1	2	122	0.26
	T9	2	108	0.27
	T7	2	93	0.28
60°C	T1	2	111	0.25
	T7	2	92	0.24

Table IV Results of Quasi-Static Fracture Tests. Comparison of Theoretical and Experimental Values of K_{Ic}.

	23°C			60°C		
HEAT TREATMENT	K_{Ic} Theoretical [MPA $\sqrt{m}$]	K_{Ic} Experimental [MPA $\sqrt{m}$]	Percent Difference	K_{Ic} Theoretical [MPA $\sqrt{m}$]	K_{Ic} Experimental [MPA $\sqrt{m}$]	Percent Difference
T1	94	75	20	88	95	7
T7	130	95	23	130	126	3
T9	82	63	26			

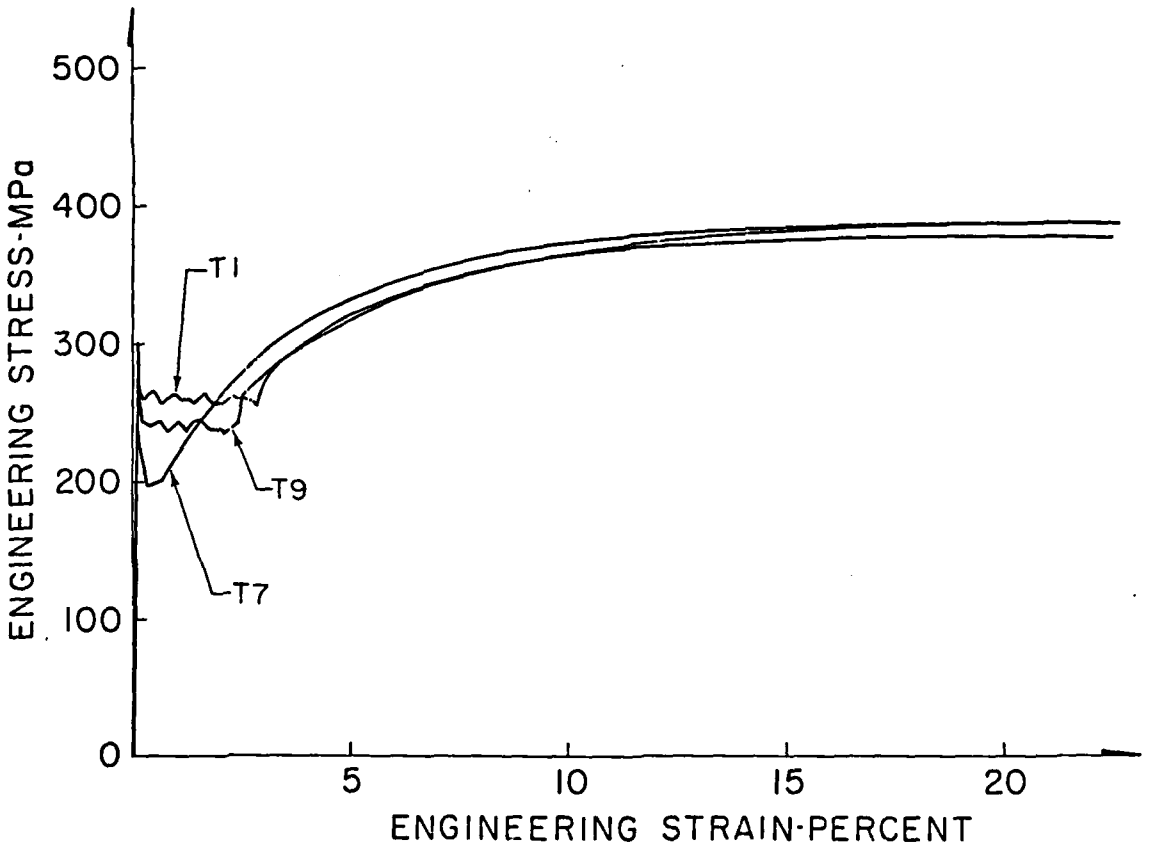

Fig. 3. Stress-Strain behavior in uniaxial tension for heat-treatments T1, T7 and T9.

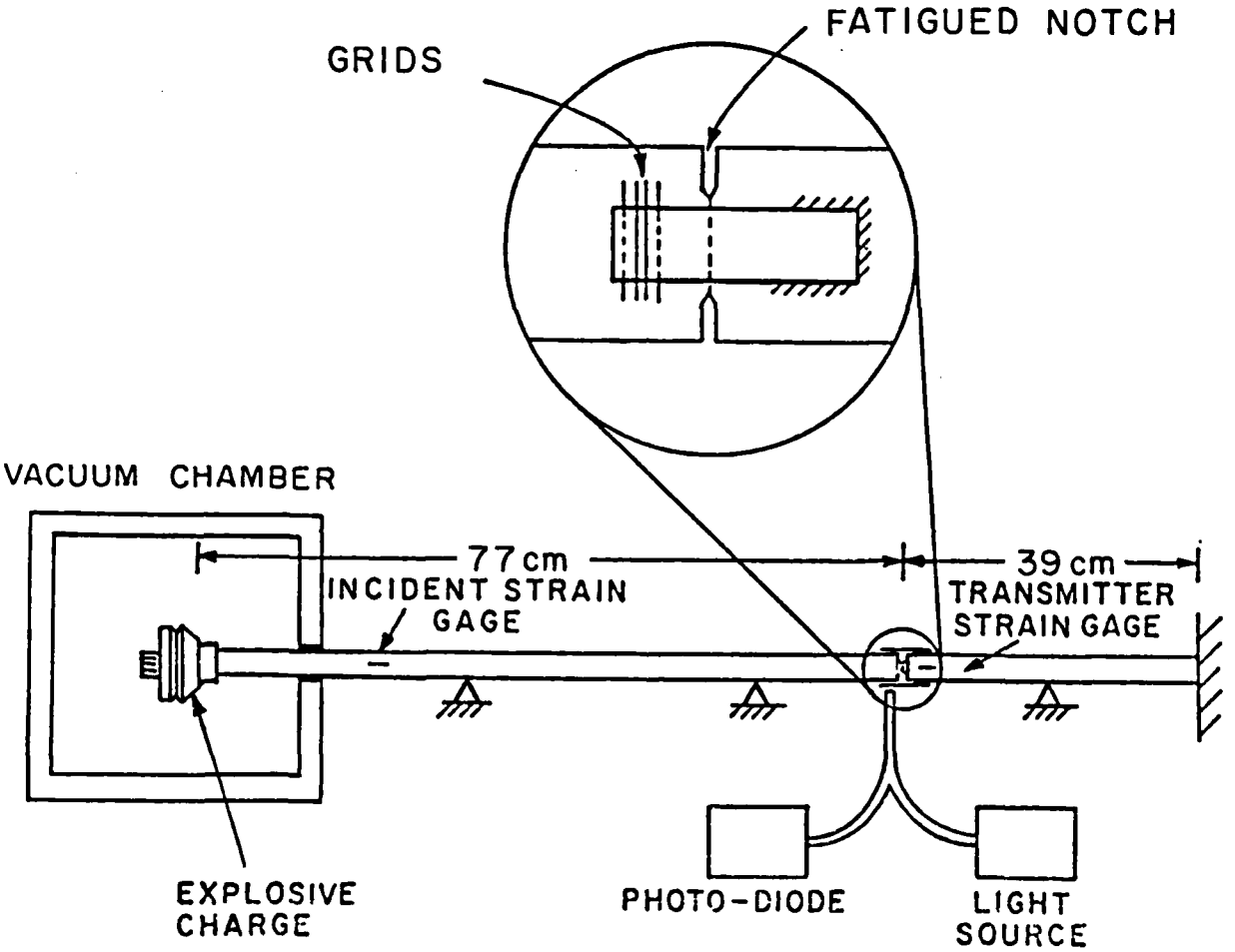

Fig. 4. Schematic diagram of apparatus for dynamic fracture initiation experiment.

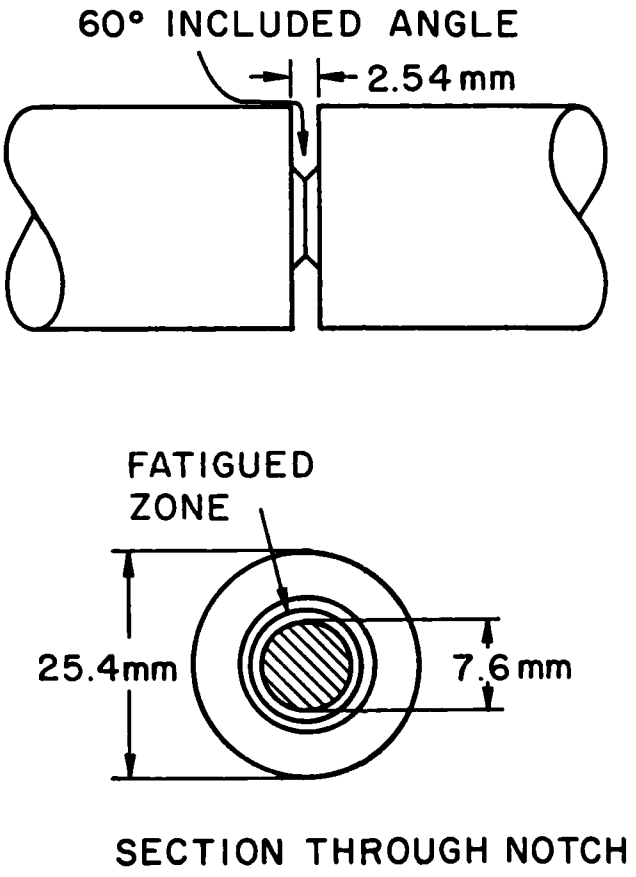

Fig. 5. Notched section of specimen, showing ligament remaining after fatigue (7.6mm diameter).

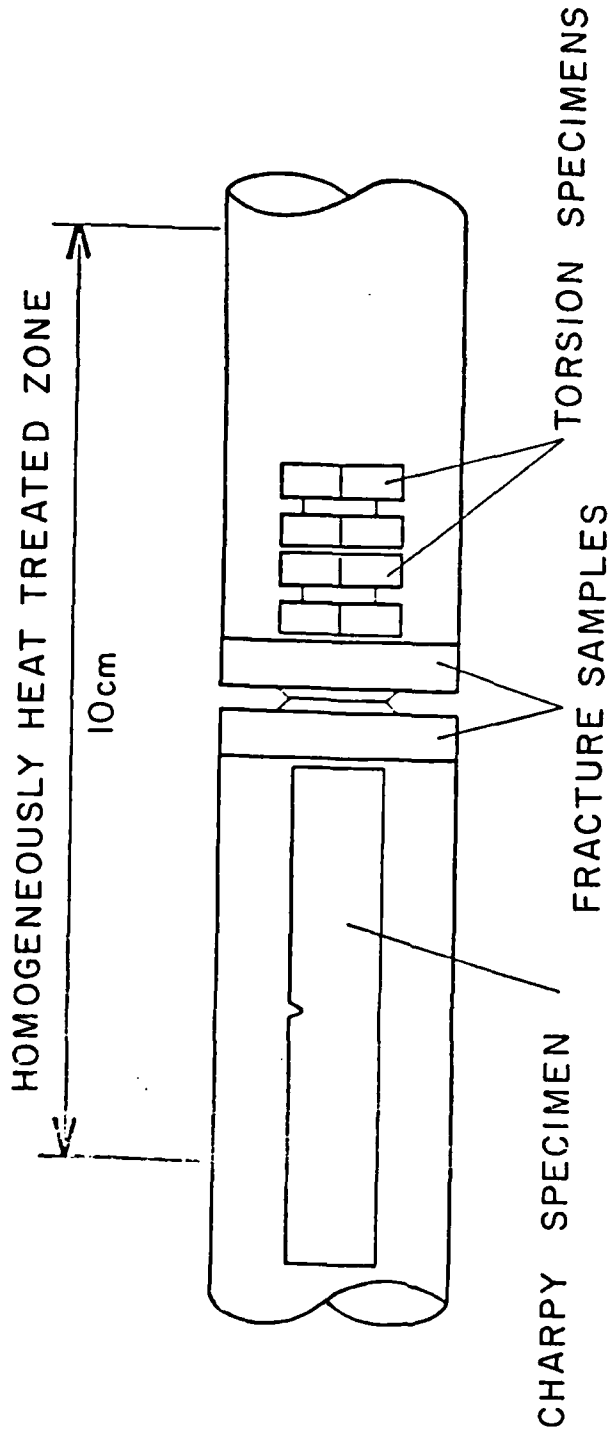

Fig. 6. Location of the torsion and Charpy specimens in the homogeneously heat-treated zone of the fracture specimen.

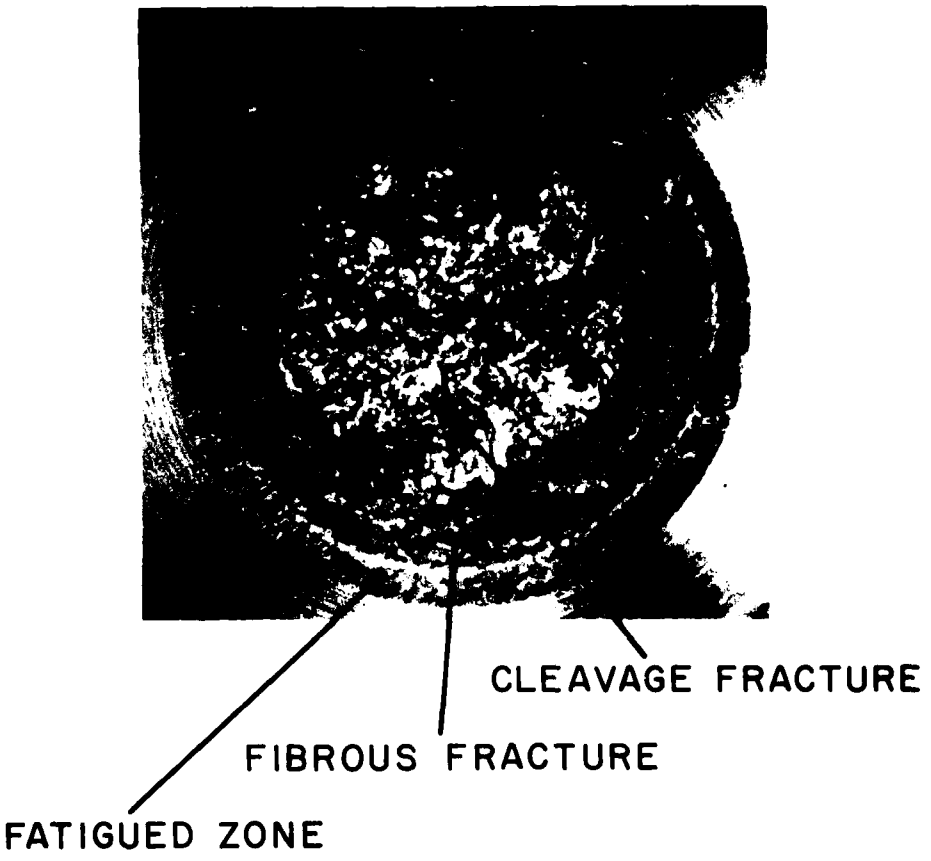

Fig. 7. Fracture surface, showing cleavage at the center surrounded by an annulus of fibrous fracture. The fatigued zone is also visible as well as part of the machined surface.

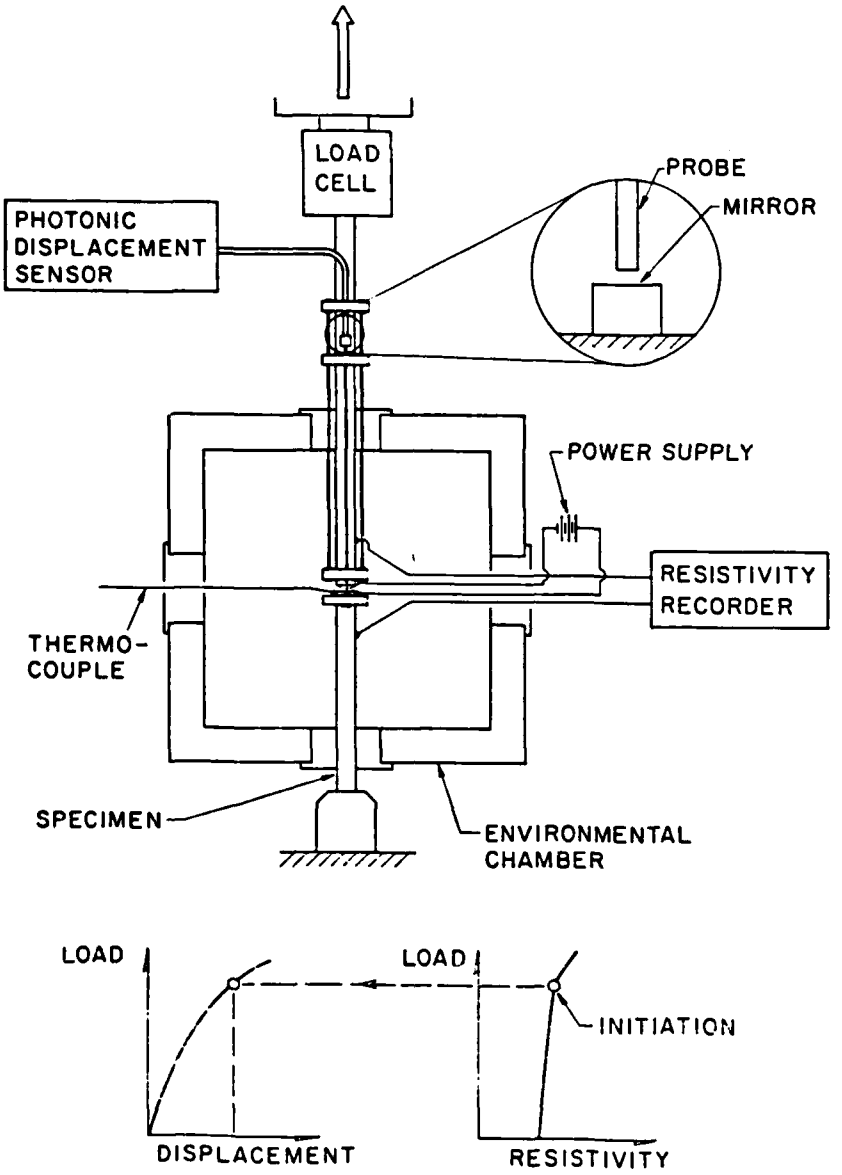

Fig. 8. Apparatus for static fracture test in Riehle testing machine. Insets show the method used to determine the COD at fracture initiation.

a) Torsional Kolsky bar

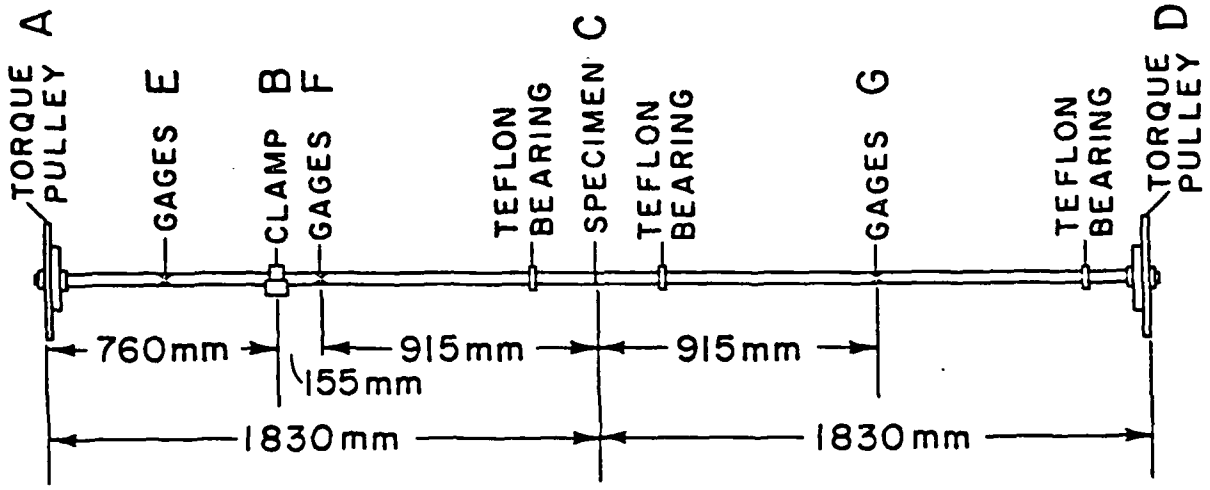

b) Torsion specimen

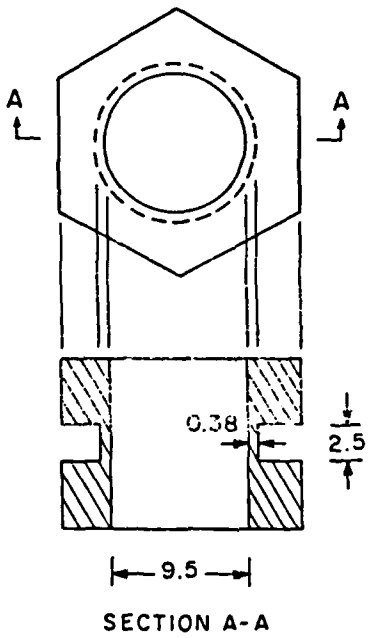

Fig. 9. Schematic diagram showing: (a) torsional Kolsky bar used to determine dynamic stress-strain properties of the steels and (b) the specimen used in this apparatus

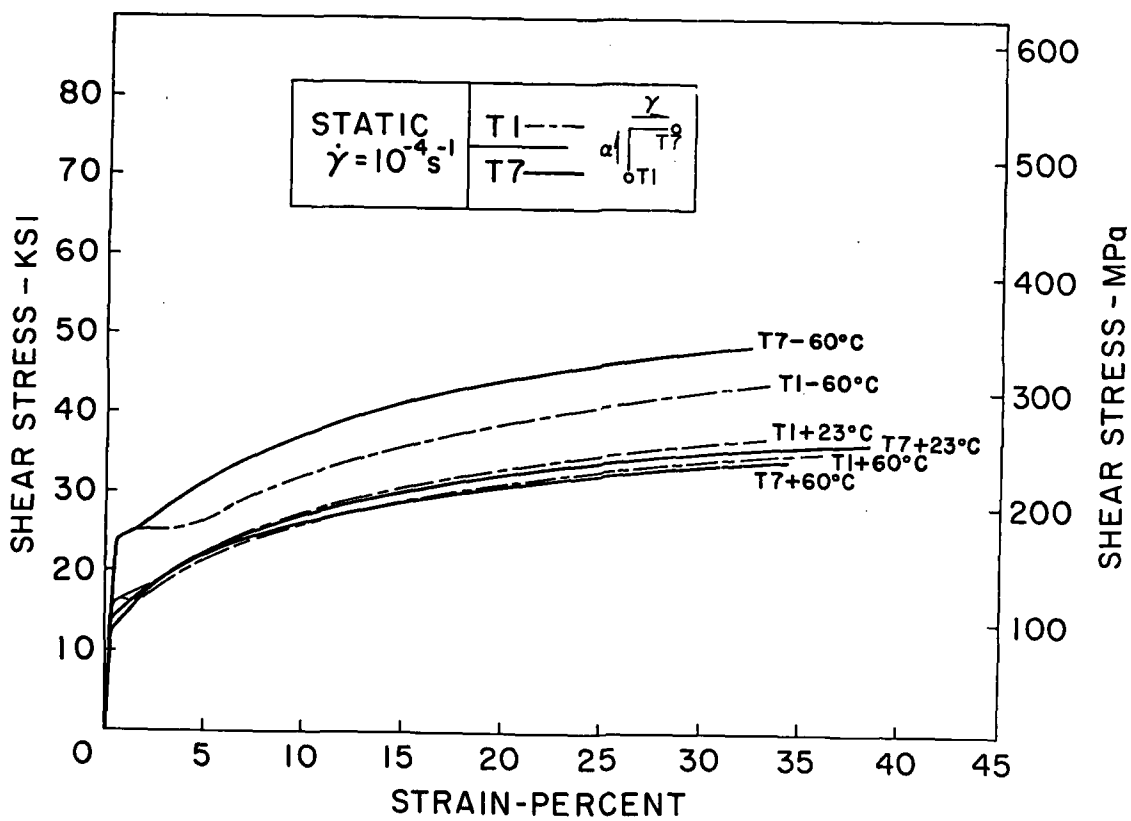

Fig. 10. Quasi-static stress-strain curves in shear for T1 and T7 microstructures.

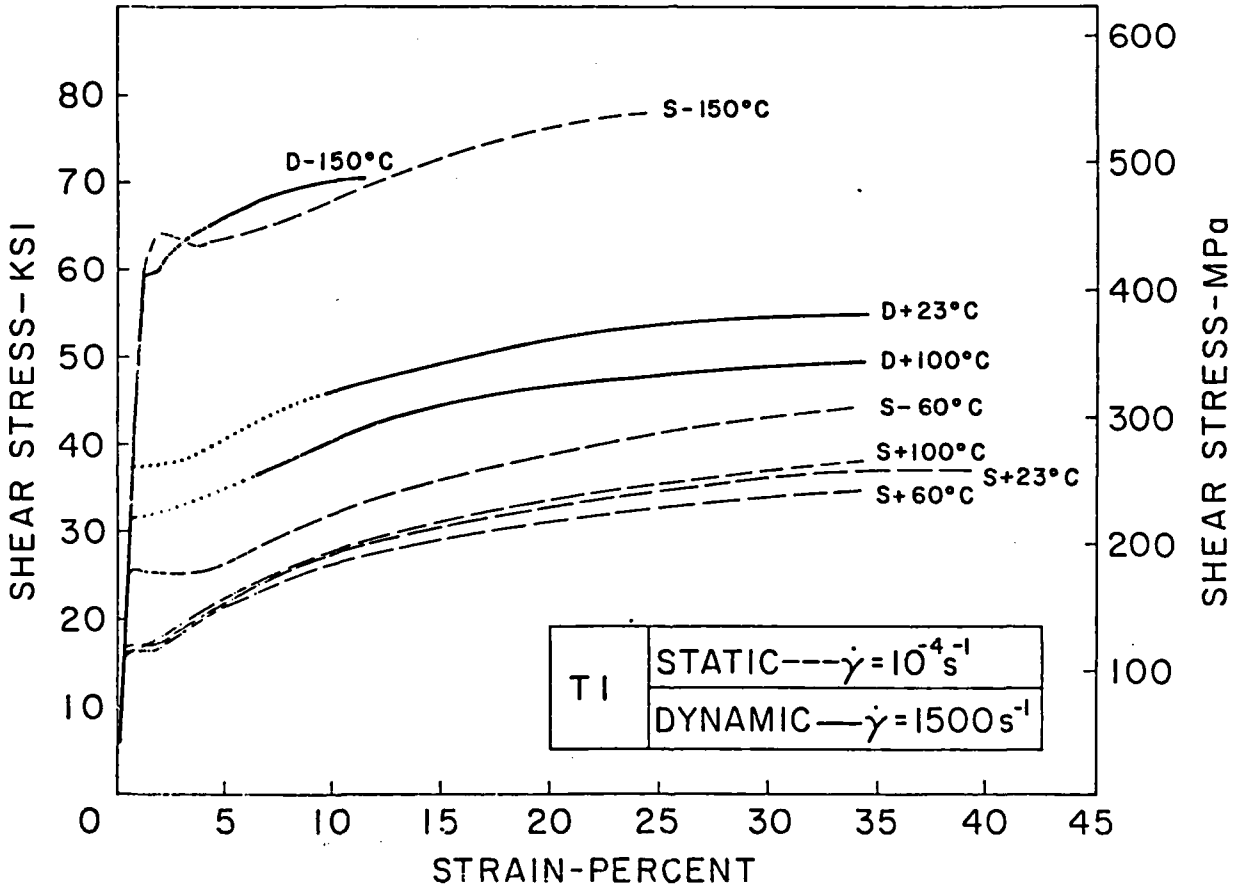

Fig. 11. Quasi-static and dynamic stress-strain curves for the finest microstructure, T1.

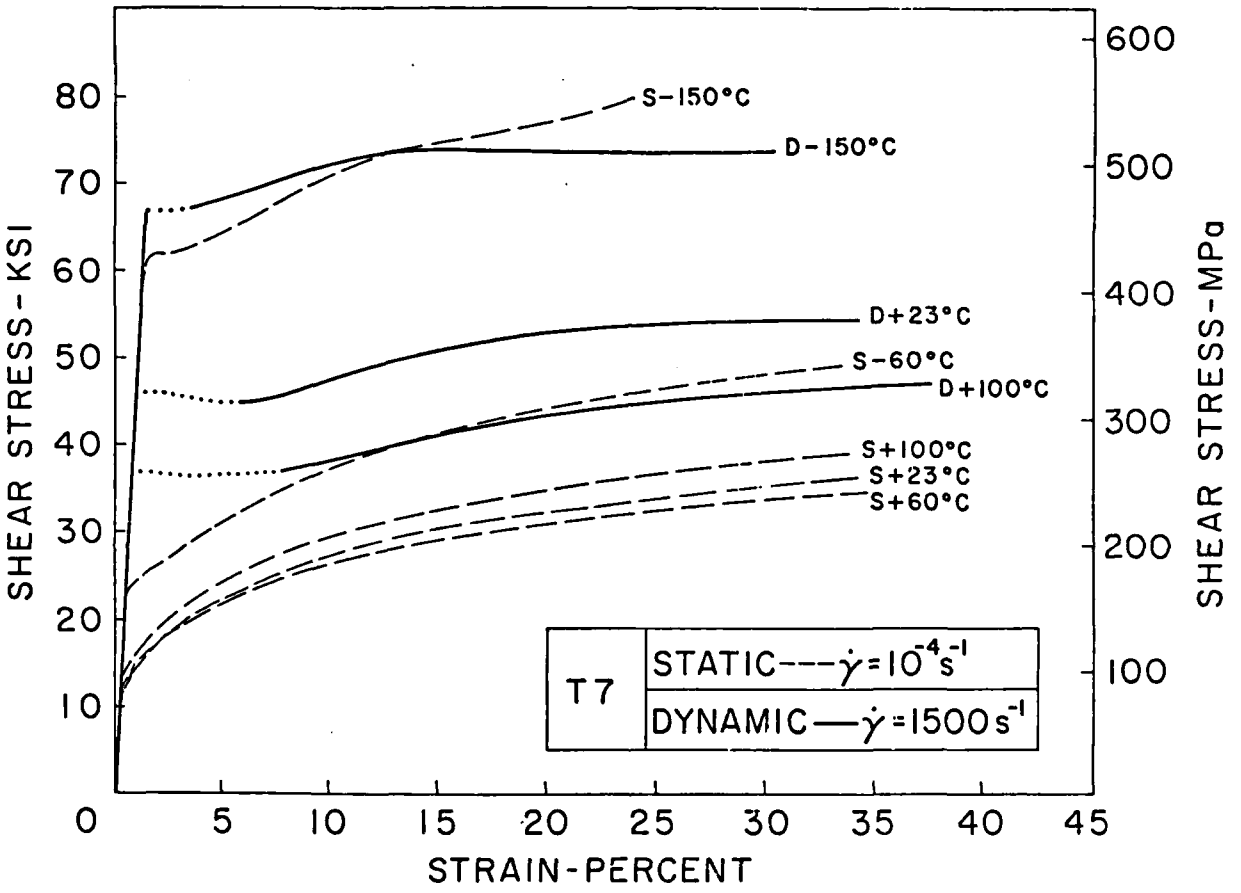

Fig. 12. Quasi-static and dynamic stress-strain curves for the coarsest microstructure, T7.

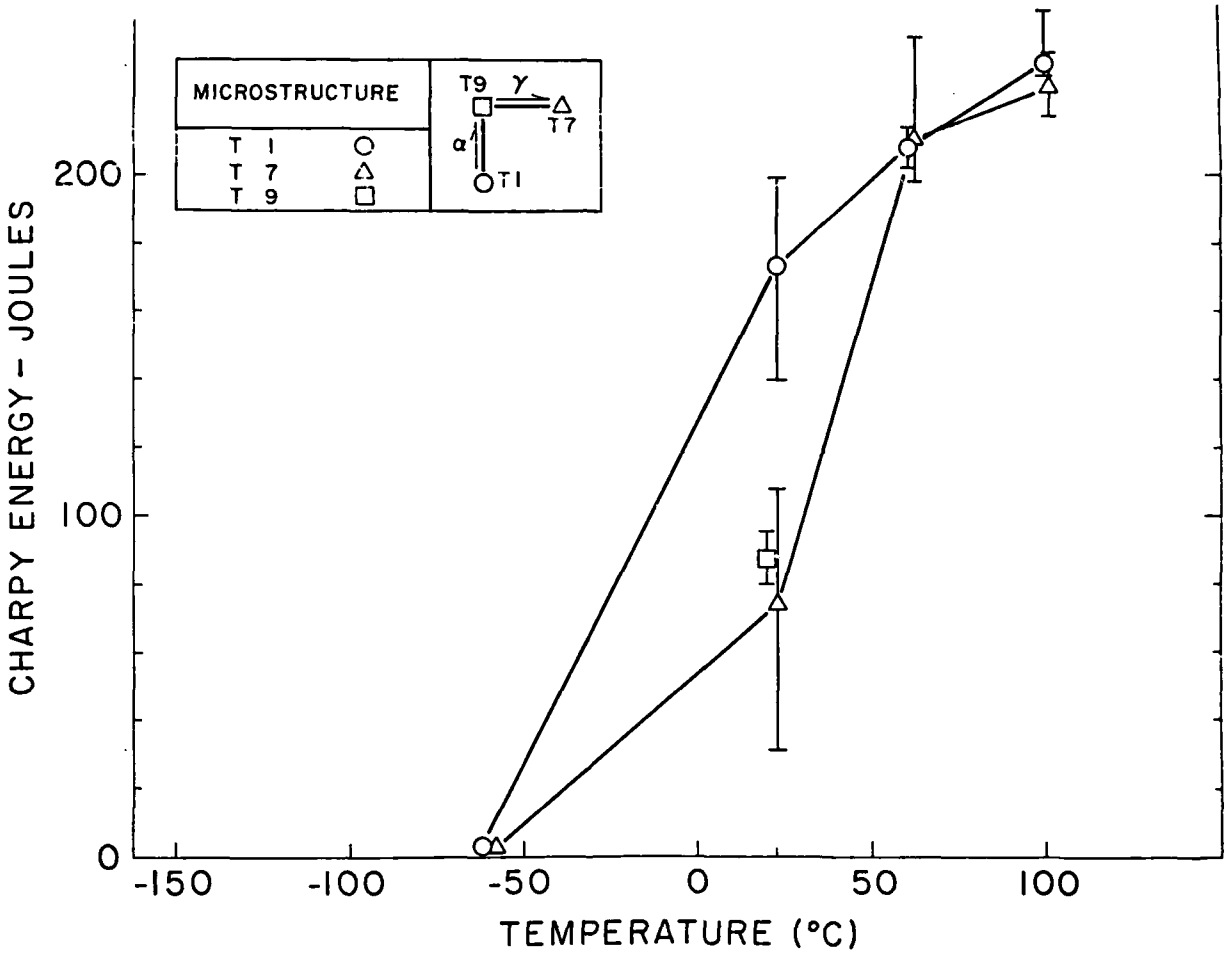

Fig. 13. Results of Charpy test for finest and coarsest microstructures T1 and T7.

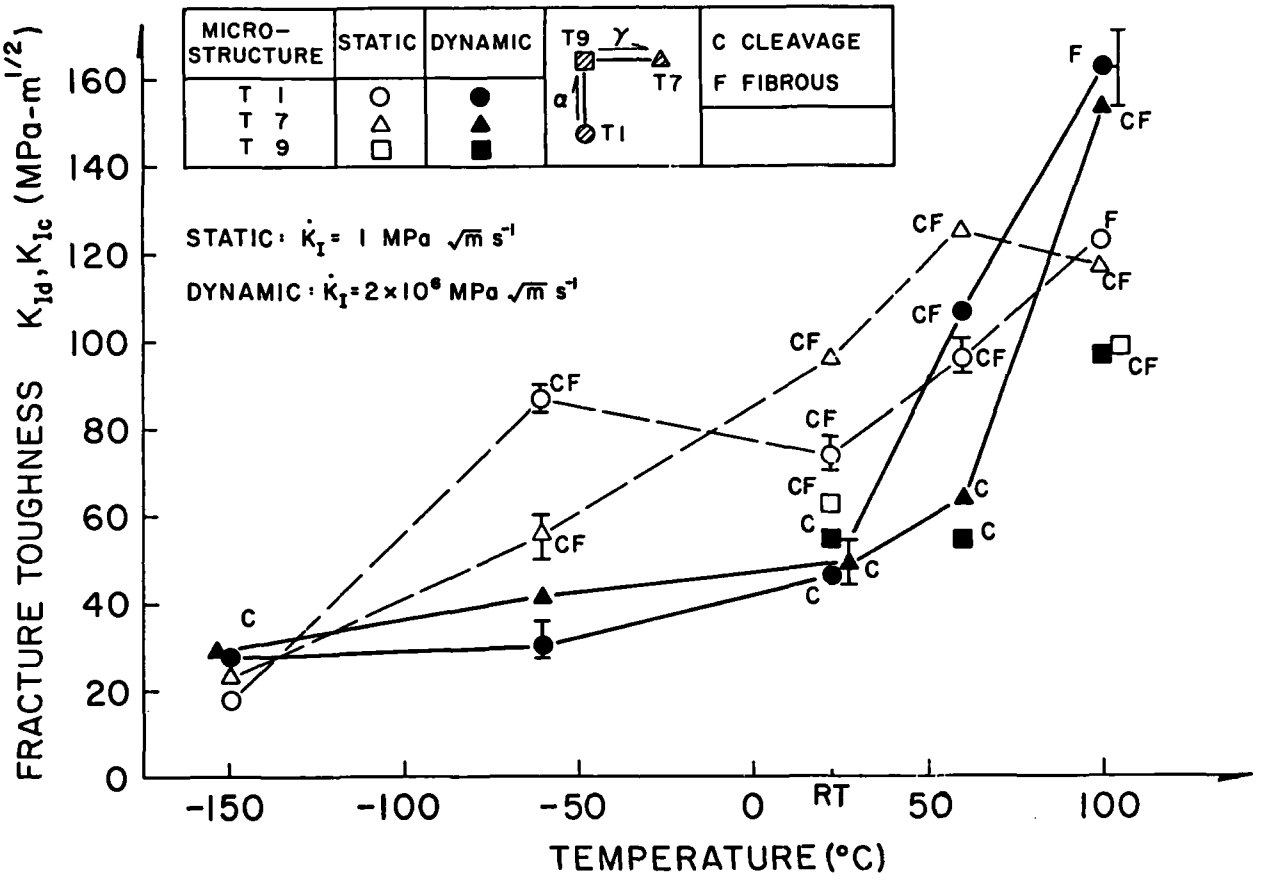

Fig. 14. Static and dynamic values of fracture toughness for the different microstructures as a function of temperature.

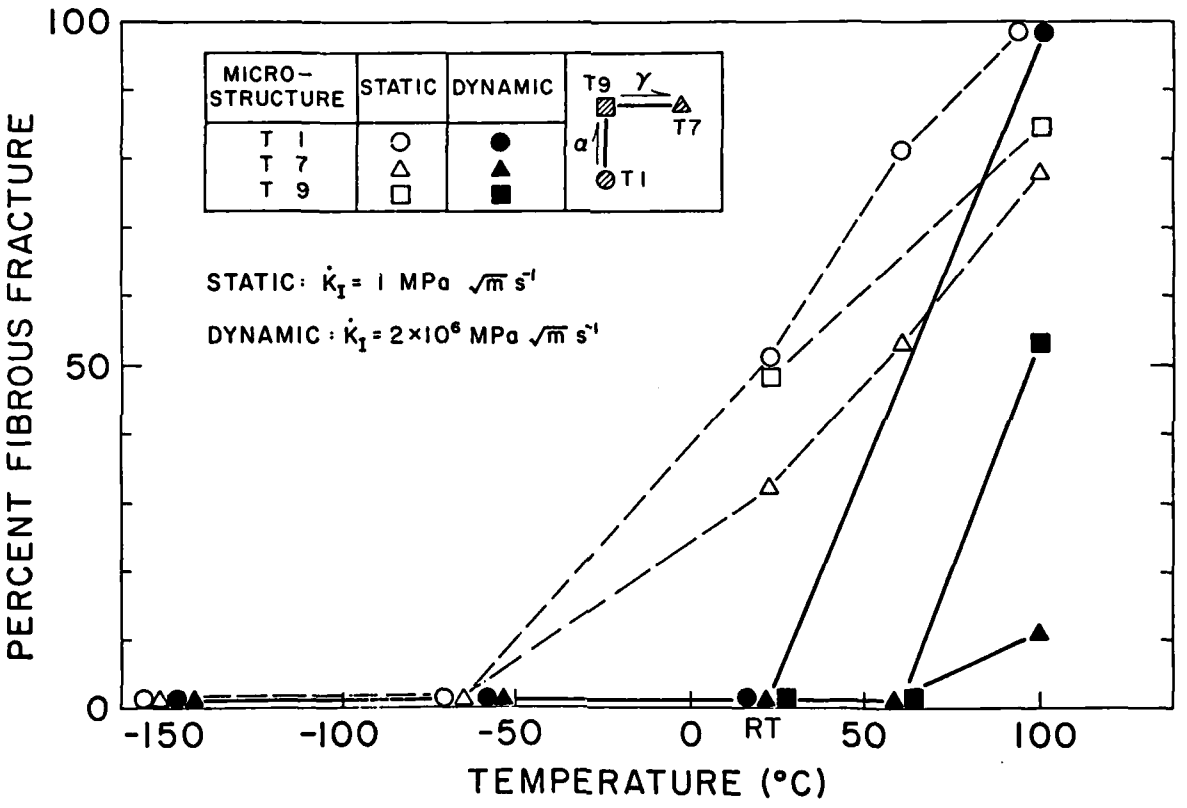

Fig. 15. Percent of fracture surface showing a fibrous appearance.

END

FILMED

10-84

DTIC